

# High energy neutrinos from radio-quiet AGNs

Jaime Alvarez-Muñiz<sup>1,2</sup> and Peter Mészáros<sup>1,3,4</sup>

<sup>1</sup>*Dept. de Física de Partículas, Universidade de Santiago de Compostela,  
15706 Santiago de Compostela, A Coruña, Spain*

<sup>2</sup>*Dept. of Astronomy & Astrophysics, Pennsylvania State University, University Park, PA 16802, USA*

<sup>3</sup>*Dept. of Physics, Pennsylvania State University, University Park, PA 16802, USA*

<sup>4</sup>*Institute for Advanced Study, Princeton, NJ 08540, USA*

Most active galactic nuclei (AGN) lack prominent jets, and show modest radio emission and significant X-ray emission which arises mainly from the galactic core, very near from the central black hole. We use a quantitative scenario of such core-dominated radio-quiet AGN, which attributes a substantial fraction of the X-ray emission to the presence of abortive jets involving the collision of gas blobs in the core. Here we investigate the consequences of the acceleration of protons in the shocks from such collisions. We find that protons will be accelerated up to energies above the pion photoproduction threshold on both the X-rays and the UV photons from the accretion disk. The secondary charged pions decay, producing neutrinos. We predict significant fluxes of TeV-PeV neutrinos, and show that the AMANDA II detector is already constraining several important astrophysical parameters of these sources. Larger cubic kilometer detectors such as IceCube will be able to detect such neutrinos in less than one year of operation, or otherwise rule out this scenario.

PACS numbers: 98.54.Cm, 95.85.Ry, 98.70.Sa

## I. INTRODUCTION

Around 90% of all active galactic nuclei (AGN), such as quasars and Seyfert galaxies, are radio-quiet, i.e. their radio emission is relatively modest. This is due to the lack of prominent jets which provide most of the radio emission in the remaining 10% of AGNs classified as radio-loud. Both types of AGN are also strong X-ray emitters, and the ultimate energy source is thought to derive from accretion of gas onto a central massive black hole (e.g. see [1]). The high energy photon emission in radio-loud jet-dominated sources such as Blazars is largely due to non-thermal processes in the jet, whose dimensions extend well beyond the outer edge of the galaxy. In radio-quiet AGNs, on the other hand, the short X-ray variability timescales as well as spectral analysis of Fe X-ray lines indicate that the emission arises in the galactic core, very near from the central black hole. Both types of AGN have been considered as possible sources of high energy cosmic rays and neutrinos (see e.g. [2] and refs. therein). Here we concentrate on the more numerous radio-quiet AGN as a source of high energy neutrinos.

The typical model of radio-quiet AGN X-ray emission is based on UV photons from the accretion disk suffering repeated inverse Compton scatterings in a hotter corona, leading to a power law X-ray spectrum (e.g. [3]). This generic model does not allow for recent evidence indicating that, at some level, many radio-quiet AGN show weak radio emission, and in rare cases even show a weak incipient radio jet. A quantitative model which attempts to provide a bridge between the two classes of AGN considers the high energy emission in the core of radio-quiet AGNs due to the presence of an abortive jet [4]. These could arise from an outflow from the inner edge of the accretion disk, similar to that inferred in radio-loud objects, but whose velocity is smaller than the escape ve-

locity from the central black hole region. As in successful jets, the outflow is expected to be intermittent, leading to shells or blobs ejected from the central region. In this case, due to their lower velocity, they will reach a maximum distance from the hole before falling back, occasionally colliding with subsequently ejected, outgoing blobs. The X-ray emission in this model is attributed to Inverse Compton scattering of UV photons from the accretion disk by electrons accelerated in the sub-relativistic shocks resulting from blob-blob collisions.

Here we consider the consequences of the acceleration of protons in the same shocks which accelerate the electrons. We find that protons will be accelerated up to energies above the energy threshold for pion photoproduction on both the X-rays produced by the accelerated electrons, as well as on the UV photon field from the accretion disk. The charged pions decay producing neutrinos. A natural outcome of this model is then the production of a flux of high energy (TeV-PeV) neutrinos, which may be detectable with  $\sim \text{km}^3$  volume detectors such as Icecube [5]. Radio-quiet AGN constitute the main bulk of AGNs, and on average can be found closer to Earth. Also, since the neutrinos are produced in sub-relativistic shocks the emission is isotropic and the aborted jets need not point towards the Earth in order for the neutrinos to be detectable. We stress, however, that our conclusions are not restricted to this specific model of aborted jets, although it is used here as a framework. Qualitatively similar results might in principle be expected in disk-corona or other AGN models, if magnetic reconnection (e.g. [6]) or shocks associated with the accretion process (e.g. [7],[8]) lead to proton acceleration near the central black hole.

In this paper we first show in Sec. II that protons can be accelerated up to  $E_p^{max} \approx 10^9$  GeV in the blob-blob collision shocks. We discuss proton interactions with X-

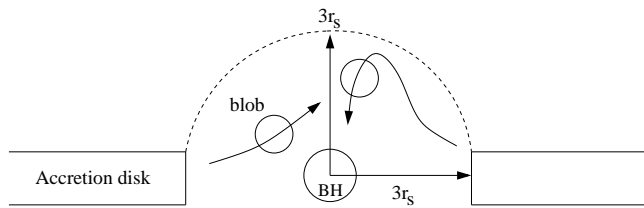


FIG. 1: Sketch of the geometry of a radio-quiet AGN core adopted in this work, showing the  $10^8 M_\odot$  black hole (BH), accretion disk and two blobs moving in opposite directions which are about to collide.  $r_s \approx 2.95 \times 10^{13}$  cm is a Schwarzschild radius for a  $10^8 M_\odot$  black hole.

rays, UV photons and cold unaccelerated protons in Sec. III. In Sec. IV we discuss neutrino production by photomeson and  $pp$  interactions, and we estimate the neutrino flux from a typical radio-quiet quasar as well as the cumulative diffuse neutrino flux from all the radio-quiet quasars in the Universe. We also calculate in this section the muon and shower event rate expected in Gigaton Cherenkov detectors such as Icecube. In Sec.V we summarize the paper and discuss the implications of our findings.

## II. PROTON ACCELERATION AND COOLING TIMES

We adopt here a nominal set of parameters which serve as a specific example for the purposes of normalization. We consider an AGN with a  $10^8$  solar mass black hole and with an accretion disk inner edge at a distance of about  $3r_s$  from the black hole, where  $r_s = 2GM/c^2 \approx 2.95 \times 10^{13}$  cm is the Schwarzschild radius (Fig. 1). We assume that blobs are ejected with an initial velocity  $\beta_0 = 0.5$ , which corresponds to a Lorentz factor  $\Gamma_0 \sim 1.15$ , i.e. they are non-relativistic and we assume that  $\Gamma_0 \sim 1$  from now on, and hence we do not make any distinction between the comoving (blob) frame and the observer's frame. The size of a blob is  $r_{\text{blob}} \approx \alpha_r r_s$  with  $\alpha_r \sim 1$ . The lifetime of the shock produced in a blob-blob collision is roughly equal to the blob-blob crossing time,  $t_{\text{cross}} \approx \alpha_r r_s / c \beta_0 \approx 2.0 \times 10^3$  s.

The Eddington luminosity of a  $10^8 M_\odot$  black hole AGN is  $L_{\text{Edd}} = 4\pi GMm_p c / \sigma_T \approx 1.26 \times 10^{46} L_{\text{Edd},8}$  erg s $^{-1}$ . This corresponds to an Eddington accretion rate  $\dot{M}_{\text{Edd}} = L_{\text{Edd}} / \eta c^2 \approx 2.8 M_\odot L_{\text{Edd},8} \eta_{0.08}^{-1} \text{ yr}^{-1}$ , where  $\eta = 0.08 \eta_{0.08}$ . Following [4] we assume that the accretion results in the intermittent ejection of blobs of matter. We also assume that a significant fraction  $\alpha_{bb} \sim 1$  of the observed X-ray luminosity is due to the blob-blob collisions, whose number at any given time is  $N_{bb}$ .  $N_{bb}$  can be estimated through a simple geometrical argument, from the number of blobs ( $N_{\text{blob}}$ ) that are present in the region around the BH at that given time.  $N_{\text{blob}}$  is given roughly by the ratio of the time of flight of a blob i.e. the time it takes for a blob to go upwards from the BH

and to fall back onto it,  $t_{\text{flight}} \approx 6r_s / \beta_0 c$ , to the average time between the launch of consecutive blobs  $\Delta t$ . Taking  $\Delta t \approx (1-2) r_s / c$ , a value that qualitatively accounts for the time variability of radio-quiet quasars [4], we obtain  $N_{\text{blobs}} \approx 10$ . The average number of collisions (optical depth) of a blob during its flying time is given by the ratio of the blob flying time  $t_{\text{flight}} \sim V_T^{1/3} / (\beta_0 c)$  to the mean time between blob collisions,  $V_T / (N_{\text{blob}} V_{\text{blob}}^{2/3} \beta_0 c)$ , where the volume of a blob is  $V_{\text{blob}} \approx (4/3)\pi r_s^3$  and the total volume inhabited by the blobs is  $V_T \approx (4/3)\pi (3r_s)^3$  (see Fig. 1), giving an average number of collisions per blob  $\approx 1$ . The number of blob-blob collisions at any given time is then  $1 < N_{bb} < 5$ . We then assume that the X-ray luminosity from the steady-state number  $N_{bb}$  of blob-blob collisions is equal to a fraction  $\alpha_{bb} \sim 1$  of the total X-ray luminosity  $L_X$ . Assuming  $L_X$  to be a fraction  $\alpha_{X,Ed} < 1$  of the Eddington luminosity, we combine these two factors into a single efficiency  $\alpha_X = L_X / L_{\text{Edd}}$  which we parametrize as  $\alpha_X \approx 0.01 \alpha_{0.01}$  corresponding to  $L_X \approx 10^{44}$  erg s $^{-1}$ , which is the X-ray luminosity of a nominal radio-quiet AGN [9]. All the calculations performed are parametrized by  $\alpha_X$ , which can vary in order to adjust  $L_X$  to the actual observed X-ray luminosity from a particular AGN.

Using the usual assumption that the magnetic field  $B$  in the shock is due to turbulent fields generated behind the shocks arising from the blob-blob collisions, the comoving (in the blob frame) magnetic field energy density is a fraction  $\epsilon_B$  of the post-shock proton thermal energy:

$$\frac{B^2}{8\pi} \approx \epsilon_B \rho_{\text{preshock}} c^2 \quad (1)$$

The density  $\rho_{\text{preshock}}$  should be roughly equal to the density of the accretion disk at a radius  $\approx 3r_s$ , which is given by [10],

$$\begin{aligned} \rho_{\text{preshock}} &\approx \rho_{\text{disk}}(3r_s) = \frac{\dot{M}}{4\pi(3r_s)^2 \alpha_v \sqrt{GM/3r_s}} \\ &\approx 1.5 \times 10^{-14} \alpha_{X,0.01} L_{\text{Edd},8} \eta_{0.08}^{-1} \text{ g cm}^{-3} \end{aligned} \quad (2)$$

where  $\dot{M} = \alpha_X L_{\text{Edd}} / \eta c^2$  and we have taken the viscosity  $\alpha_v \approx 0.1$  [10]. From  $\rho_{\text{preshock}}$  the proton number density is,

$$n_p = \frac{\rho_{\text{preshock}}}{m_p} \approx 8.7 \times 10^9 \alpha_{X,0.01} L_{\text{Edd},8} \eta_{0.08}^{-1} \text{ cm}^{-3} \quad (3)$$

where  $m_p$  is the proton mass. The magnetic field is then

$$\begin{aligned} B &\approx \sqrt{8\pi \epsilon_B^{1/2} \rho_{\text{preshock}}^{1/2}} \\ &\approx 1.0 \times 10^4 (\alpha_{X,0.01} L_{\text{Edd},8})^{1/2} \epsilon_{B,0.3}^{1/2} \text{ G} \end{aligned} \quad (4)$$

where  $\epsilon_B = (1/3) \epsilon_{B,0.3}$ .

The proton acceleration time is given by  $t_p^{\text{acc}} \approx A_p r_L / c$  where  $r_L$  is the Larmor radius in the magnetic field in the blob, and  $A_p$  is a constant  $\geq 1$ . Using Eq. (4) we get,

$$t_p^{\text{acc}} \approx \frac{A_p \gamma_p m_p}{eB}$$

$$\approx 9.9 \times 10^{-9} A_p (\alpha_{X,0.01} L_{edd,8})^{-1/2} \epsilon_{B,0.3}^{-1/2} \gamma_p \quad (5)$$

The proton synchrotron cooling time is

$$t_p^{syn} = \frac{6\pi m_p^3 c}{\sigma_{Th} m_e^2 \gamma_p B^2} \approx 4.4 \times 10^{10} (\alpha_{X,0.01} L_{edd,8})^{-1} \epsilon_{B,0.3}^{-1} \gamma_p^{-1} \text{ s} \quad (6)$$

where  $\sigma_{Th} \approx 0.665 \times 10^{-24} \text{ cm}^2$  is the Thomson cross section. Equating the synchrotron cooling time and the acceleration time (see Eq. (5)) we get the maximum energy of the accelerated protons,

$$E_p^{max} \approx 2.0 \times 10^9 A_p^{-1/2} (\alpha_{X,0.01} L_{edd,8})^{-1/4} \epsilon_{B,0.3}^{-1/4} \text{ GeV} \quad (7)$$

Protons can also suffer Inverse Compton (IC) losses from interactions with X-ray and UV photons from the disk. To estimate the X-ray photon number density, we take into account that the blobs are optically thin [4] so X-ray photons escape freely, and their density is  $n_X \simeq \alpha_X L_{edd} / 4\pi (3r_s)^2 c E_X$ , or

$$n_X \approx \frac{\alpha_X L_{edd} t_{cross}}{(4/3)\pi r_s^3 E_X} \approx 5.3 \times 10^{13} \alpha_{X,0.01} L_{edd,8} E_{X,\text{keV}}^{-1} \text{ cm}^{-3} \quad (8)$$

where  $E_X = 1 E_{X,\text{keV}} \text{ keV}$  is the typical energy of the emitted X-rays.

To estimate the density of UV photons from the accretion disk, we consider thermal emission in the inner disk between  $\approx 3r_s$  and  $7.5r_s$ . This portion of the disk emits an UV luminosity  $\alpha_{UV} L_{edd}$ . Observationally the X-ray luminosity is of the order of 10-50% the luminosity in the optical-UV [11]. We then take  $\alpha_{UV} \approx 5\alpha_X \approx 0.05 \alpha_{UV,0.05}$ . The equilibrium temperature (energy) of the UV photons can be approximately estimated assuming the emission from the disk follows a black-body spectrum, yielding:

$$E_{UV} \approx k_B \left( \frac{\alpha_{UV} L_{edd}}{\sigma A_{\text{disk}}} \right)^{1/4} \approx 8.3 (\alpha_{UV,0.05} L_{edd,8})^{1/4} \text{ eV} \quad (9)$$

where  $k_B$  and  $\sigma$  are Boltzmann's and Stefan-Boltzmann's constant respectively, and  $A_{\text{disk}}$  is the area of the inner disk. The number density of UV photons is then,

$$n_{UV} \approx \frac{\alpha_{UV} L_{edd}}{A_{\text{disk}} c E_{UV}} \approx 1.2 \times 10^{16} (\alpha_{UV,0.05} L_{edd,8})^{3/4} \text{ cm}^{-3} \quad (10)$$

and we get that  $n_{UV} \approx 200 n_X$ .

The inverse Compton scattering of protons on X-rays and UV photons is in the Thomson limit for energies below  $E_p^{IC}$ , where

$$E_p^{IC} \ll \frac{m_p^2}{E_{X,UV}} \approx \begin{cases} 8.8 \times 10^5 E_{X,\text{keV}}^{-1} & \text{GeV (X)} \\ 1.1 \times 10^8 (\alpha_{UV,0.05} L_{edd,8})^{-1/4} & \text{GeV (UV)} \end{cases}$$

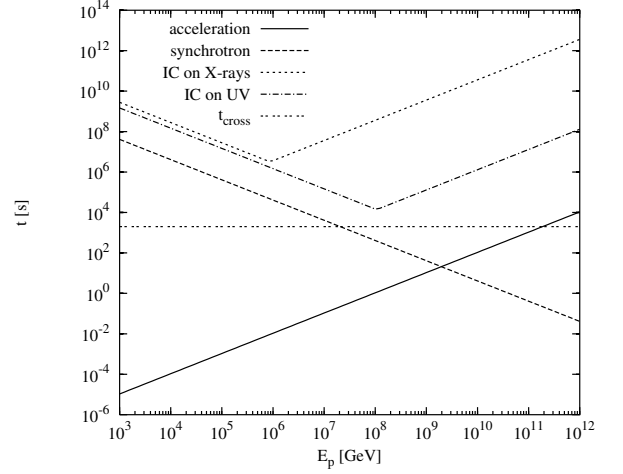


FIG. 2: Proton cooling times as a function of proton energy for different energy loss processes, namely, synchrotron and inverse Compton scattering on both X-rays and UV photons. Also shown are the proton acceleration time, and the blob-blob crossing time.

The IC cooling times on X-ray and UV photons are then, in the Thomson (Th) limit

$$t_p^{IC,Th} \approx \frac{m_p}{\sigma_{Th} (m_e/m_p)^2 c \gamma_p E_{X,UV} n_{X,UV}} \approx \begin{cases} 3.0 \times 10^{12} (\alpha_{X,0.01} L_{edd,8})^{-1} \gamma_p^{-1} \text{ s} & \text{(X)} \\ 1.6 \times 10^{12} (\alpha_{UV,0.05} L_{edd,8})^{-1} \gamma_p^{-1} \text{ s} & \text{(UV)} \end{cases}$$

and in the Klein-Nishina (KN) ( $E_p \gg E_p^{IC}$ ) limit

$$t_p^{IC,KN} \approx \frac{\gamma_p (E_\gamma/m_p)}{\sigma_{Th} (m_e/m_p)^2 c n_{X,UV}} \approx \begin{cases} 3.4 (\alpha_{X,0.01} L_{edd,8})^{-1} E_{X,\text{keV}}^{-2} \gamma_p \text{ s} & \text{(X)} \\ 1.2 \times 10^{-4} (\alpha_{UV,0.05} L_{edd,8})^{-1/2} \gamma_p \text{ s} & \text{(UV)} \end{cases}$$

In Fig. 2 we show the IC cooling times on X-rays and UV photons along with the synchrotron cooling and the proton acceleration times as a function of proton energy. Also shown is the dynamic (blob-blob crossing) time. It can be seen that IC losses and adiabatic losses (given by the crossing time) do not impose any constraints on the maximum proton energy, which is dominantly restricted by the synchrotron energy losses, and is given in Eq. (7).

### III. PROTON INTERACTIONS

High energy protons accelerated in the blob-blob collision shock can interact with X-rays produced in the shocks, UV photons in the disk or cold (unaccelerated) protons in the blobs. The proton threshold energy for photomeson production on X-rays and UV photons at the  $\Delta$ -resonance is given by  $E_p E_\gamma \approx 0.3 \text{ GeV}^2$  which yields,

$$E_{p,th}^X \approx 3.0 \times 10^5 E_{X,\text{keV}}^{-1} \text{ GeV} \quad (11)$$

for photomeson production on X-rays, and

$$E_{p,th}^{UV} \approx 3.6 \times 10^7 (\alpha_{UV,0.05} L_{Edd,8})^{-1/4} \text{ GeV} \quad (12)$$

for interactions on UV photons.

The threshold for inelastic  $pp \rightarrow pn\pi^+$  interactions in which neutrinos can be produced is much smaller and is given by,

$$E_{p,th}^p = \frac{(m_p + m_n + m_\pi)^2 - 2m_p^2}{2m_p} \approx 1.23 \text{ GeV} \quad (13)$$

The optical depth for photomeson interactions on X-rays, from Eq. (8), is

$$\tau_{p\gamma}^X \approx r_s (\sigma_{p\gamma \rightarrow \Delta}) n_X \approx 7.8 \times 10^{-1} \alpha_{X,0.01} L_{Edd,8} E_{X,keV}^{-1} \quad (14)$$

and the corresponding optical depth on UV photons, from Eq. (10), is,

$$\tau_{p\gamma}^{UV} \approx r_s (\sigma_{p\gamma \rightarrow \Delta}) n_{UV} \approx 1.8 \times 10^2 (\alpha_{UV,0.05} L_{Edd,8})^{3/4} \quad (15)$$

where  $\sigma_{p\gamma \rightarrow \Delta} \approx 5 \times 10^{-28} \text{ cm}^2$  is the photomeson production cross section at the  $\Delta$ -resonance.

Protons can also interact with cold (unaccelerated) protons in the blob. We assume that a fraction  $\xi_p < 1$  of the protons are Fermi accelerated in the shocks produced in the blob-blob collisions. The  $pp$  collisions should dominate below  $E_{p\gamma,th}^X$ , the energy threshold for photomeson production on X-rays. In this energy range the mean total cross-section for  $pp$  interactions is  $\langle \sigma_{pp} \rangle \approx 6 \times 10^{-26} \text{ cm}^2$ , roughly two orders of magnitude larger than the photomeson production cross section and the density of proton targets is typically  $10^3$  times smaller than the X-ray density, resulting from Eq. (3) in a smaller optical depth for the  $L_X \approx 10^{44} \text{ erg s}^{-1}$  adopted here,

$$\begin{aligned} \langle \tau_{pp} \rangle &\approx \langle \sigma_{pp} \rangle r_s (1 - \xi_p) n_p \\ &\approx 1.5 \times 10^{-2} (1 - \xi_p) \alpha_{X,0.01} L_{Edd,8} \eta_{0.08}^{-1} \quad (16) \end{aligned}$$

This is the optical thickness for accelerated protons encountering blob thermal nucleons. In addition, accelerated protons emitted in some directions will also collide with inner disk thermal nucleons. If the disk inner edge is at  $3r_s$  and has a thickness  $3r_s$ , a fraction  $2\pi(3r_s)^2/(4\pi(3r_s)^2) \sim (1/2)$  will collide with nucleons in the inside wall of the accretion disk, for which  $\tau_{pp}$  is larger due to the larger path length available. The density at inner edge is comparable to the blob density, and varies with radius, while the effective path length depends on the incidence angle. We adopt as an estimate for the average proton incident on the disk a value of  $\tau_{pp} \sim 10$  times larger than in a blob.

Inverse Compton scattering of protons on X-rays or UV photons does not affect the  $p\gamma$  scattering rate, since the optical depth for IC scattering  $\tau_{IC} < 10^{-1} \tau_{p\gamma}$  for all target photons and in both the Thomson and Klein-Nishina regimes.

The ratio of IC to  $pp$  optical depth in the Thomson regime ( $E_p < E_p^{IC}$ ) is

$$\begin{aligned} \frac{\tau_{IC}}{\langle \tau_{pp} \rangle} &= \frac{\sigma_{Th} n_{X,UV} (m_e/m_p)^2}{\langle \sigma_{pp} \rangle (1 - \xi_p) n_p} \quad (17) \\ &\approx \begin{cases} 2.0 \times 10^{-2} (1 - \xi_p)^{-1} E_{X,keV}^{-1} & \text{(X)} \\ 4.6 (1 - \xi_p)^{-1} \alpha_{X,0.01}^{-1} \alpha_{UV,0.05}^{3/4} L_{Edd,8}^{-1/4} & \text{(UV)} \end{cases} \end{aligned}$$

and hence  $pp$  interactions which are dominant below the energy threshold for photomeson production on X-rays, are suppressed by IC scattering on UV photons for the  $L_X \approx 10^{44} \text{ erg s}^{-1}$  and  $L_{UV} \approx 5 \times 10^{44} \text{ erg s}^{-1}$  of the nominal radio-quiet quasar. In the Klein-Nishina regime  $\tau_{IC}/\langle \tau_{pp} \rangle$  is lower than above, however in this regime  $p\gamma$  interactions dominate as we will see below.

### A. $p\gamma$ interactions on a power-law X-ray spectrum

High energy neutrinos are produced in  $p\gamma$  interactions with both X-rays and UV photons above the corresponding energy thresholds  $E_{p\gamma,th}^X \approx 3.0 \times 10^5 \text{ GeV}$  and  $E_{p\gamma,th}^{UV} \approx 3.6 \times 10^7 \text{ GeV}$  respectively. However, the X-ray spectra of AGN, including the radio-quiet, are typically of power-law form, and hence protons at energies below  $E_{p\gamma,th}^X$  can also produce delta resonances by interacting with photons from the high energy tail of the X-ray spectrum. The same is true for  $p\gamma$  interactions with UV photons in which low energy protons can photoproduce on photons from the high energy tail of the blackbody photon distribution. As a first approximation, we will neglect the tail of the blackbody distribution, and assume that the UV spectrum is monoenergetic. However, we will take into account that the X-ray spectrum follows a power-law given by  $dN_\gamma/dE_\gamma \propto E_\gamma^{-\delta}$ . As a consequence the optical depth to  $p$ -X-rays depends on the spectral index  $\delta$  of the photon spectrum, as well as on proton energy. This is due to the fact that as  $E_p$  increases, protons interact with an increasing number of lower energy photons. For a steep X-ray spectrum, the bulk of the X-ray photons are concentrated in the low energy region of the power-law distribution, and this increases the optical depth to  $p$ -X-ray interactions for high energy protons. For a photon number density spectrum  $\propto E^{-\delta}$ , the energy dependent optical depth is given by,

$$\tau_{p\gamma}^X(E_\gamma) \simeq r_s (\sigma_{pX \rightarrow \Delta}) E_\gamma \frac{dn_\gamma}{dE_\gamma} \propto E_\gamma^{1-\delta} \quad (18)$$

Using the threshold relation  $E_p E_\gamma \approx 0.3 \text{ GeV}^2$  Eq. (18) turns into,

$$\begin{aligned} \tau_{p\gamma}^X(E_p) &\simeq \tau_{p\gamma}^X(E_\gamma = 1 \text{ keV}) \left( \frac{E_p}{E_{p,th}^X} \right)^{\delta-1} \\ &\approx 7.8 \times 10^{-1} (\alpha_{X,0.01} L_{Edd,8}) \left( \frac{E_p}{E_{p,th}^X} \right)^{\delta-1} \quad (19) \end{aligned}$$

where  $\tau_{p\gamma}^X(E_\gamma = 1 \text{ keV}) := \tau_{p\gamma}^{X,\text{keV}}$  is the optical depth given in Eq. (14). The factor  $(E_p/E_{p,th}^X)^{(\delta-1)}$  accounts for the increasing optical depth as  $E_p$  increases (note that this is only for  $\delta > 1$ , which is observationally the case).

From the discussion above, it follows that (for  $\delta > 1$ ) there is a proton energy  $E_p^c$  above which photoproduction on X-rays dominates over photoproduction on UV photons. The energy  $E_p^c$  is given by the condition  $\tau_{p\gamma}^X(E_p^c) = \tau_{p\gamma}^{\text{UV}}$ . Solving for  $E_p^c$  we have

$$E_p^c = \left[ \frac{\tau_{p\gamma}^{\text{UV}}}{\tau_{p\gamma}^{X,\text{keV}}} \right]^{1/(\delta-1)} E_{p,th}^X$$

$$\approx [229.6 \alpha_{X,0.01}^{-1} \alpha_{\text{UV},0.05}^{3/4} L_{\text{Edd},8}^{-1/4}]^{1/(\delta-1)} E_{p,th}^X \quad (20)$$

The predominant target for  $p\gamma$  interactions is determined by the numerical value of  $E_p^c$  and whether it is larger or smaller than  $E_{p,th}^{\text{UV}}$ , the energy above which  $p$ 's photoproduce on UV photons, as well as by its relative value with respect to  $E_p^{\text{max}}$ , the maximum energy of the accelerated protons.  $E_p^c$  depends on the X-ray spectral index  $\delta$ . It follows that:

- If  $\delta \geq \delta_c \approx 2.13$  then  $E_p^c \leq E_{p,th}^{\text{UV}}$ , implying that proton interactions with X-rays photons always dominate over interactions with UV photons.
- If  $1 < \delta \leq \delta_l \approx 1.61$  then  $E_p^c \geq E_p^{\text{max}}$  and interactions with X-rays dominate up to  $E_{p\gamma,th}^{\text{UV}}$ , while photoproduction on UV photons dominates above  $E_{p\gamma,th}^{\text{UV}}$ .
- If  $\delta_l < \delta < \delta_c$  there is a small proton energy range above  $E_{p\gamma,th}^{\text{UV}}$  but below  $E_p^{\text{max}}$  in which photoproduction on UV photons dominates, whereas interactions with X-rays are more important outside it.

The numerical value of  $\delta_c$  is obtained from the condition  $E_p^c(\delta_c) = E_{p,th}^{\text{UV}}$  whereas  $\delta_l$  is obtained from the equation  $E_p^c(\delta_l) = E_p^{\text{max}}$ . They depend on the particular values of  $L_X$  and  $L_{\text{UV}}$ . The situation is illustrated in Fig. 3, where  $E_p^c$  is plotted as a function of  $\delta$ , along with  $E_p^{\text{max}}$  and  $E_{p\gamma,th}^{\text{UV}}$ . The dark grey shaded area represents the region in the space parameter of  $(E_p, \delta)$  where interactions on X-rays are dominant, while photoproduction on UV photons is more important in the light gray shaded area. Interactions above  $E_p^{\text{max}}$  (unshaded region) are not possible, since protons do not get accelerated to  $E_p > E_p^{\text{max}}$ .

For the  $pp$  interactions, similarly to the discussion above, there is a proton energy  $E_p^{\text{pp}}$  below which  $pp$  interactions are more important than interactions with X-rays, given by the condition  $\tau_{p\gamma}^X(E_p^{\text{pp}}) = \langle \tau_{pp} \rangle$ . Solving for  $E_p^{\text{pp}}$  we get:

$$E_p^{\text{pp}} = \left[ \frac{\langle \tau_{pp} \rangle}{\tau_{p\gamma}^{X,\text{keV}}} \right]^{1/(\delta-1)} E_{p,th}^X$$

$$\approx [9.8 \times 10^{-3}]^{1/(\delta-1)} E_{p,th}^X \quad (21)$$

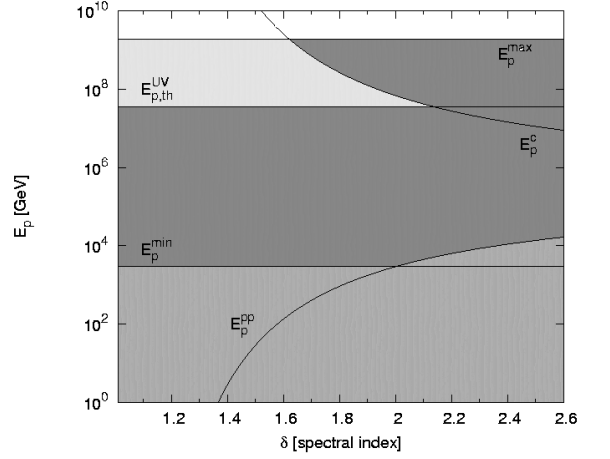


FIG. 3: Several energy scales relevant for proton interactions for the set of parameters of the nominal radio-quiet quasar:  $M_{\text{BH}} = 10^8 M_\odot$ ,  $\alpha_{X,0.01} = 1$ ,  $\alpha_{\text{UV},0.05} = 1$ .  $E_p^{\text{max}}$  is the maximum energy for proton acceleration.  $E_{p,th}^{\text{UV}}$  is the proton energy threshold for photomeson production on UV photons.  $E_p^{\text{min}}$  is the lowest energy of a proton that can interact through the  $\Delta$ -resonance with an X-ray assuming the maximum X-ray energy is  $E_\gamma^{\text{max}} = 100 \text{ keV}$ . The upper curve is  $E_p^c$ , the energy above which the optical depth for  $p\gamma$  interactions on X-rays is larger than the corresponding optical depth on UV photons. The lower curve is  $E_p^{\text{pp}}$  the energy below which the  $pp$  optical depth is larger than the  $p\gamma$  optical depth on X-rays.  $p\gamma$  interactions on X-rays are dominant in the darkest gray shaded parameter space region  $(E_p, \delta)$ .  $p\gamma$  interactions on UV photons dominate in the lightest gray shaded area, whereas  $pp$  interactions are more important in the medium gray shaded region at the bottom of the plot.

There is also another important energy scale,  $E_\gamma^{\text{max}}$  which is the photon energy above which the source runs out of energetic enough X-rays to interact with protons of energy below  $E_p^{\text{min}}$  given by the photoproduction threshold condition:  $E_p^{\text{min}} E_\gamma^{\text{max}} \approx 0.3 \text{ GeV}^2$ . Observationally, most radio-quiet AGN spectra show an X-ray cut-off at about 100-150 keV. We will adopt  $E_\gamma^{\text{max}} = 100 \text{ keV}$  in this work.

As in the case of  $p\gamma$  interactions,  $E_p^{\text{pp}}$  depends on the index of the X-ray spectrum. For a steep enough spectrum there are not enough high energy photons to interact with low energy protons and then  $pp$  interactions dominate below a proton energy larger than  $E_p^{\text{min}}$ . This occurs for  $\delta \geq \delta_p \sim 2.00$  given by  $E_p^{\text{pp}}(\delta_p) = E_p^{\text{min}}$ , using  $\xi_p = 0.5$  and the standard set of luminosities of the nominal radio-quiet AGN. This is also shown in Fig. 3 where  $E_p^{\text{pp}}$  is plotted along with  $E_p^{\text{min}}$  assuming  $E_\gamma^{\text{max}} = 100 \text{ keV}$ . Thus,  $pp$  interactions dominate in the medium gray region at the bottom of Fig. 3 if the  $p$  flux is not suppressed by IC scattering, which depends on the luminosity of the source.

#### IV. NEUTRINO PRODUCTION AND DETECTION

High energy neutrinos are produced through secondary charged  $\pi$  decay photoproduced in  $p\gamma \rightarrow \Delta$  and  $n\gamma \rightarrow \Delta$  interactions. Each of the 4 leptons produced in the charged pion decay chain  $\pi^\pm \rightarrow \mu\nu_\mu \rightarrow e\nu_e\nu_\mu\bar{\nu}_\mu$  carry about 1/4 of the initial pion energy.

Neutrinos can also be produced through pion and muon decay produced in  $pp$  interactions in the shocks. In fact  $pp$  interactions are dominant at low proton energies (medium-grey shaded region at the bottom of Fig.3). The typical neutrino energy is 1/4 of the initial pion energy, and this is determined by the pion multiplicity in the  $pp$  collisions.

Due to the high magnetic field and dense photon environment where the  $\pi^+$  and  $\mu^+$  are produced, they might lose their energies through synchrotron and inverse Compton scattering before decaying to neutrinos.

The synchrotron cooling time for pions and muons is calculated using Eq. (6). The charged pion and muon decay times are  $\tau_\pi^{dec} \approx 2.6 \times 10^{-8} \gamma_\pi$  s, and  $\tau_\mu^{dec} \approx 2.2 \times 10^{-6} \gamma_\mu$  s. Equating the synchrotron cooling time and the decay time, we get the synchrotron break energies above which neutrino production is suppressed by a factor  $\propto E_\nu^{-2}$  due to energy losses:

$$E_\pi^{sb} \approx 1.0 \times 10^7 (\alpha_{X,0.01} L_{Edd,8})^{-1/2} \epsilon_{B,0.3}^{-1/2} \text{ GeV} \quad (22)$$

for pions, and,

$$E_\mu^{sb} \approx 5.6 \times 10^5 (\alpha_{X,0.01} L_{Edd,8})^{-1/2} \epsilon_{B,0.3}^{-1/2} \text{ GeV} \quad (23)$$

for muons.

Inverse Compton scattering on both X-rays and UV photons does not contribute significantly to the pion and muon energy loss. For all photon targets and in both the Thomson and Klein-Nishina regimes, the inverse Compton cooling time is at least  $\approx 10$  times larger than the decay times (and much larger than this  $\approx 10^2 - 10^7$  in most cases) and hence we ignore pion and muon IC scattering energy losses in the calculation of the neutrino flux.

##### A. Neutrino flux from the nominal radio-quiet quasar

Protons are accelerated by the Fermi mechanism in the blob-blob shocks up to energies  $E_p^{max} \approx 10^9$  GeV, following an energy spectrum  $\propto E_p^{-2}$ . The energy per unit time given to protons producing neutrinos is,

$$\int_{E_p^{th}}^{E_p^{max}} E_p \frac{d^2 N_p}{dE_p dt} dE_p = \xi_p \alpha_X L_{Edd} \quad (24)$$

Taking  $d^2 N_p / dE_p dt = K_p / E_p^2$  we get for  $K_p$ ,

$$K_p \approx 3.2 \times 10^{45} \frac{\xi_p \alpha_{X,0.01} L_{Edd,8}}{\ln(E_p^{max}/E_p^{th})} \text{ GeV s}^{-1} \quad (25)$$

The proton fluence per unit time is,

$$F_p = \frac{1}{4\pi D_L^2} E_p^2 \frac{d^2 N}{dE_p dt} \quad (26)$$

$$\approx 1.6 \times 10^{-5} \frac{\xi_p \alpha_{X,0.01} L_{Edd,8}}{D_{L,1}^2 \ln(E_p^{max}/E_p^{th})} \frac{\text{GeV}}{\text{cm}^2 \text{s}}$$

for a source at a luminosity distance  $D_L = 1 D_{L,1}$  Mpc.

##### 1. Neutrino flux from $p\gamma$ interactions

The neutrino flux for each neutrino flavor is given by,

$$\Phi_\nu^{p\gamma} = \frac{1}{4} f_\pi F_p \quad (27)$$

$$\times \begin{cases} E_\nu^{-2} & ; E_{\nu,th}^{sb} < E_\nu < E_\nu^{sb} \\ E_\nu^{-2} (E_\nu^{sb}/E_\nu)^2 & ; E_\nu^{sb} < E_\nu < E_\nu^{max} \end{cases}$$

where  $E_\nu^{sb} \approx (1/4) E_\pi^{sb}$  for muon neutrinos produced in  $\pi$  decays, and  $E_\nu^{sb} \approx (1/4) E_\mu^{sb}$  for electron and muon neutrinos produced in the decay of  $\mu$ 's.  $E_\pi^{sb}$  and  $E_\mu^{sb}$  are given in Eqs. (22) and (23) respectively,  $E_{\nu,th}^{sb} = 0.05 E_{p,th}^{sb}$  and  $E_\nu^{max} = 0.05 E_p^{max}$ .

$f_\pi$  is the fraction of proton energy given to pions. As discussed in subsection III A,  $f_\pi$  depends on proton energy (and hence on neutrino energy) and on  $\delta$  the spectral index of the X-ray energy distribution, which determine the dominant photon target (X-rays or UV photons). For interactions on X-rays  $f_\pi$  is given by,

$$f_\pi^X = \min \left[ 1, \langle x_{p \rightarrow \pi} \rangle \tau_{p\gamma}^{X,keV} \left( \frac{E_\nu}{E_{\nu,th}^X} \right)^{\delta-1} \right] \quad (28)$$

where  $\langle x_{p \rightarrow \pi} \rangle \approx 0.2$  is the average inelasticity in a  $p\gamma$  interaction,  $\tau_{p\gamma}^{X,keV}$  is given in Eq. (14) and  $E_{\nu,th}^X = 0.05 E_{p\gamma,th}^X$  given in Eq. (11). For interactions on UV photons,

$$f_\pi^{UV} = \min(1, \langle x_{p \rightarrow \pi} \rangle \tau_{p\gamma}^{UV}) \quad (29)$$

where  $\tau_{p\gamma}^{UV}$  is given in Eq. (15).

The dependence of  $f_\pi$  on  $\delta$  and  $E_\nu$  can be summarized as follows,

- If  $\delta \geq \delta_c$ , then:

$$f_\pi = f_\pi^X; \quad E_{\nu,th}^X < E_\nu < E_\nu^{max} \quad (30)$$

- If  $1 < \delta \leq \delta_l$ , then:

$$f_\pi = \begin{cases} f_\pi^X; & E_\nu < E_{\nu,th}^{UV} \\ f_\pi^{UV}; & E_{\nu,th}^{UV} < E_\nu < E_\nu^c \\ f_\pi^X; & E_\nu > E_\nu^c \end{cases} \quad (31)$$

where  $E_{\nu,th}^{UV} \approx 0.05 E_{p\gamma,th}^{UV}$  given in Eq. (12), and  $E_\nu^c \approx 0.05 E_p^c$  given in Eq. (20).

- If  $\delta_l < \delta < \delta_c$ , then:

$$f_\pi = \begin{cases} f_\pi^X; & E_\nu < E_{\nu,th}^{UV} \\ f_\pi^{UV}; & E_\nu > E_{\nu,th}^{UV} \end{cases} \quad (32)$$

## 2. Neutrino flux from $pp$ interactions

The neutrino flux from  $pp$  interactions is [12]

$$\Phi_\nu^{pp} = \frac{1}{2} \int f_{pp,1} M_\nu(E_p) \frac{F_p}{E_p^2} dE_p \quad (33)$$

$$+ \frac{1}{2} \int f_{pp,2} M_\nu(E_p) \frac{F_p}{E_p^2} dE_p \quad (34)$$

for  $E_p < E_{p,th}^p$ , where  $f_{pp,1} = \min(1, \langle \tau_{pp} \rangle)$ , and  $f_{pp,2} = \min(1, 10 \langle \tau_{pp} \rangle)$  accounting for the larger optical depth in the inner wall of the accretion disk where  $\sim 1/2$  of the accelerated protons interact (see Section III).  $M_\nu(E_p)$  is the neutrino multiplicity through pion decay in the  $pp$  interactions which can be parameterized as [13],

$$M_\nu(E_p) = \frac{7}{4} \left( \frac{E_\nu}{\text{GeV}} \right)^{-1} \left[ \frac{1}{2} \ln \left( \frac{10^{11} \text{ GeV}}{E_p} \right) \right]^{-1} \\ \times \Theta \left( \frac{1}{4} \frac{m_\pi}{\text{GeV}} \gamma_{\text{CM}} \leq \frac{E_\nu}{\text{GeV}} \leq \frac{1}{4} \frac{E_p}{\text{GeV}} \right) \quad (35)$$

for each neutrino flavor.

Figure 4 shows the neutrino flux produced in  $pp$  and  $p\gamma$  interactions, for the nominal radio-quiet quasar at a distance  $D_L = 20$  Mpc. The quasar X-ray spectrum is fairly universal, typically being  $E_\gamma^{-\delta}$  with  $\delta = 1.7$  [14]. For this spectral index and for the nominal radio-quiet quasar, interactions with unaccelerated protons, X-rays and UV photons contribute to the neutrino flux (see Fig. 3). Below the proton threshold for interaction on X-rays,  $pp$  interactions dominate neutrino production, however  $pp$  collisions are largely suppressed due to the more dominant inverse Compton scattering on UV photons (see Eq. 18). This behavior continues until the protons have enough energy to interact with the high energy tail of the X-ray photon spectrum. This effect accounts for the rapid increase in the neutrino flux around  $\approx 200$  GeV seen in Fig. 4. After that the flux is slightly flatter than the expected  $E_\nu^{-2}$  power law due to the  $E_\nu^{\delta-1} = E_\nu^{0.7}$  factor in the  $\tau_{p\gamma}^X$  optical depth. As energy increases  $f_\pi$  reaches 1 and the neutrino flux goes as  $E_\nu^{-2}$ , before synchrotron losses by pions become important making the neutrino flux to fall as  $E_\nu^{-4}$ .

The normalization as well as the shape of the neutrino flux changes with luminosity. This is illustrated in Fig. 4 for a radio-quiet quasar of  $L_X \approx 10^{45}$  erg s $^{-1}$  and  $M_{\text{BH}} = 10^8 M_\odot$ . For larger  $L_X$  the optical depth to  $pX$ -rays interactions reaches 1 at a smaller proton (and hence neutrino) energy due to the denser photon target, and as a consequence the  $E_\nu^{-2}$  behavior of the spectrum starts at a lower energy than in the nominal AGN. Besides, since for fixed black hole mass, the pion synchrotron break energies scales as  $L_X^{-1/2}$  (see Eq. (22)) the flux starts to fall as  $E_\nu^{-4}$  at a lower energy than for the lower luminosity AGN.

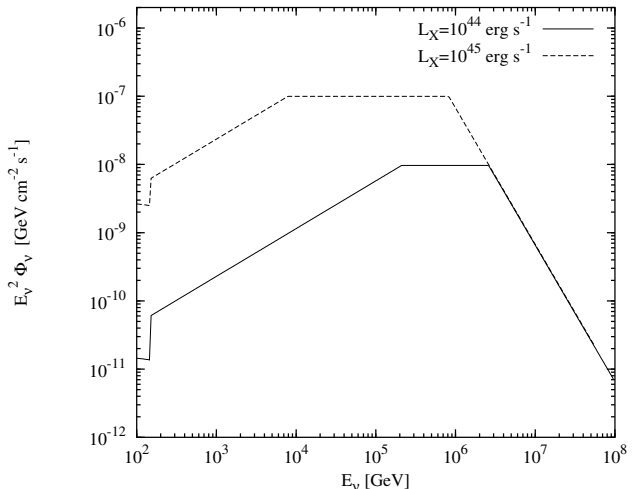


FIG. 4: Solid line: Neutrino flux reaching Earth for the nominal radio-quiet quasar:  $M_{\text{BH}} = 10^8 M_\odot$ ,  $\alpha_X = 0.01$  ( $L_X \approx 10^{44}$  erg s $^{-1}$ ) and  $\alpha_{\text{UV}} = 0.05$  at a luminosity distance  $D_L = 20$  Mpc,  $(1+z) \approx 1$ . Dashed line: Neutrino flux for a set of parameters  $M_{\text{BH}} = 10^8 M_\odot$ ,  $\alpha_X = 0.1$  ( $L_X \approx 10^{45}$  erg s $^{-1}$ ) and  $\alpha_{\text{UV}} = 0.5$  at  $D_L = 20$  Mpc. Only  $\nu_\mu$  from pion decay produced in  $pp$  and  $p\gamma$  interactions are shown in the figure.

## B. Diffuse neutrino flux

The cumulative neutrino flux from all radio-quiet AGNs in the Universe is obtained by convolution of the observed point source neutrino flux with the luminosity function taking into account its cosmological evolution,

$$\Phi_{\nu,\text{ob}}^{\text{diff}}(E_{\nu,\text{ob}}) = \frac{1}{4\pi} \int_{L_{\text{min}}}^{L_{\text{max}}} dL_X \int_0^{z_{\text{max}}} dz \frac{dn_0}{dL_X} f(z) \frac{dV}{dz} \Phi_{\nu,\text{ob}} \quad (36)$$

where  $dn_0/dL_X$  describes the present day X-ray luminosity function of the sources and  $f(z)$  is its cosmological evolution. We have used the broken power-law luminosity and evolution functions of reference [9] (model I). In a Friedmann-Robertson-Walker universe the comoving volume element is  $dV/dz = 4\pi D_L^2 c |dt/dz| / (1+z)$  and the derivative of the cosmic time  $t$  with respect to redshift  $z$  is  $(dt/dz)^{-1} = -H_0(1+z) \sqrt{(1+\Omega_m z)(1+z)^2 - \Omega_\Lambda(2z+z^2)}$  where we have used a standard  $\Lambda$ CDM cosmology with  $\Omega_m = 0.3$  and  $\Omega_\Lambda = 0.7$ . The neutrino energy in the observer's frame and the source frame are related by  $E_\nu = E_{\nu,\text{ob}}(1+z)$ , and the luminosity at the source is  $(1+z)^2$  the luminosity observed today. In the integration we take into account that the shape of the observed individual neutrino spectrum depends on the luminosity of the source as illustrated in Fig. 4.

We have performed the calculation of the diffuse flux in two different ways. First we assume that in all the individual sources the same fraction of the Eddington luminosity ( $\alpha_X = 0.01$ ) is converted to X-rays, adjusting

the mass of the black hole in order to get the necessary X-ray luminosity (variable  $M_{\text{BH}}$  case). As an alternative calculation, we assume the black hole has the same mass in all sources ( $M_{\text{BH}} = 10^8 M_{\odot}$ ) and we vary the efficiency of conversion of Eddington luminosity into X-rays, i.e. we vary  $\alpha_X$ , adjusting its value so that we get the required  $L_X$  (fixed  $M_{\text{BH}}$  case).

In Fig. 5 we plot the diffuse  $\nu_{\mu} + \bar{\nu}_{\mu}$  flux as obtained in both calculations. The contribution to the total neutrino flux from radio-quiet AGNs in different luminosity bins is shown. The less luminous AGNs, although more abundant, do not contribute much to the total because the neutrino flux scales with luminosity. The most luminous sources, although powerful neutrino emitters, are less abundant and contribute very little to the total flux.

In the case of fixed black hole mass (bottom panel) the dimensions of the accretion disk and black hole region are also fixed, and as luminosity increases the density of protons and X-rays increases linearly with  $L_X$ . Proton interactions with X-rays start to become important at an increasingly smaller energy as  $L_X$  increases due to the denser X-ray target. At the same time, the synchrotron break occurs at an increasingly lower energy because the magnetic field increases as  $L_X^{1/2}$  (see Eq. (4)). The two effects are visible in Fig. 5.

In the case of variable  $M_{\text{BH}}$  (top panel), an increase in luminosity for a fixed accretion efficiency is accompanied by an increase of the black hole mass, i.e. the accretion disk and black hole region becomes larger, and the proton and photon density actually decrease as  $M_{\text{BH}}^{-1}$ . This has the effect of decreasing the magnetic field intensity in the source and hence the synchrotron break occurs at larger energy as  $L_X$  increases. However the optical depth to  $p\gamma$  interactions stays the same as  $M_{\text{BH}}$  increases and as a consequence the proton energy at which it reaches 1, i.e. the energy at which the neutrino flux starts falling as  $E_{\nu}^{-2}$ , stays the same. The two effects are again visible in the top panel of Fig. 5.

Using Eq. (19) one sees that for low luminosity AGNs,  $L_X < 10^{41} \text{ erg s}^{-1}$ ,  $\tau_{p\gamma}^X < 1$  for all proton energies up to  $E_p^{\text{max}}$ , and protons can escape from the sources contributing to the observed cosmic ray spectrum. As a consequence, neutrinos produced in the blob-blob shocks in low luminosity AGNs would in principle be affected by the Waxman-Bahcall bound:  $E_{\nu}^2 dN_{\nu}/dE_{\nu} < (1-4) \times 10^{-8} \text{ GeV cm}^{-2} \text{ s}^{-1}$  [18]. However, the contribution of sources with  $L_X < 10^{41} \text{ erg s}^{-1}$  to the total neutrino flux is in any case below the Waxman-Bahcall bound, as can be seen in Fig. 5, while for larger luminosities, the neutrinos are produced in regions where the optical depth to  $p\gamma$  collision is typically  $\geq 1$ . Thus the Waxman-Bahcall bound does not apply to the sources considered here.

Also shown in Fig. 5 are the latest AMANDA II limits on  $\nu_{\mu} + \bar{\nu}_{\mu}$  for an  $E_{\nu}^{-2}$  diffuse flux [15, 16] which apply in different energy ranges, as well as the expected IceCube sensitivity (90% C.L.) after 1 year of operation for an  $E_{\nu}^{-2}$  flux [5]. The energy range in which the IceCube sensitivity is shown, is for illustrative purposes only.

It is important to remark that the nominal muon event rates (see below), as well as the individual source and diffuse neutrino fluxes of figures 4 and 5 are proportional to  $\alpha_{bb}$  (the fraction of the X-ray flux in radio-quiet AGN which is due to a core component) and to  $\xi_p$  (the fraction of protons which is accelerated in core shocks of any origin, attributed here more specifically to blob-blob collisions). The values adopted here as an example,  $\alpha_{bb} \sim 1$  and  $\xi_p \sim 0.5$ , are reasonable but not well constrained so far. Additional uncertainties for the diffuse neutrino flux are the approximate luminosity function, and the fraction of radio-quiet AGNs (which may be thought of as an average  $\alpha_{bb}$ ) for which a core X-ray component requires invoking shocks, blob collisions, aborted jets or other mechanisms besides an accretion disk. The AMANDA II neutrino detector is currently sensitive to the diffuse neutrino fluxes predicted here with the above parameters (see Fig. 5), and hence gives important information about the relevant astrophysical parameters of the aborted jets scenario, namely, that the product  $\alpha_{bb} \times \xi_p$  may be a factor  $\lesssim 1/2$  times the nominal values adopted here. The larger  $\text{km}^3$  IceCube will be able to detect the diffuse fluxes in less than 1 year of operation, or otherwise rule out the generic model explored in this paper.

### C. Event rate in a Gigaton telescope

We estimate here the neutrino event rate from a single nearby radio-quiet AGN, taking as an example a distance  $D_L \approx 20 \text{ Mpc}$ , comparable to that of the Virgo cluster of galaxies. We assume the nominal radio-quiet AGN with parameters:  $M_{\text{BH}} = 10^8 M_{\odot}$ ,  $\alpha_{\text{UV},0.05} = 1$ , and  $\alpha_{\text{X},0.01} = 1$ , i.e.  $L_X \sim 10^{44} \text{ erg s}^{-1}$ . Considering neutrinos from  $p\gamma$  interactions, the energy in neutrinos reaching the Earth per unit area and time from a source at this distance, from Eqs. (27) and (28), is  $F_{\nu} \approx 10^{-8} \text{ GeV cm}^{-2} \text{ s}^{-1}$ , where we have used  $\xi_p = 0.5$ ,  $f_{\pi} = 1$ ,  $E_p^{\text{max}} = 2 \times 10^9 \text{ GeV}$  and  $E_{p,\text{th}}^p = 1.23 \text{ GeV}$ . The number of neutrinos reaching the Earth assuming a typical neutrino energy  $E_{\nu} = 100 \text{ TeV} = 10^5 \text{ GeV}$  is  $\approx F_{\nu}/E_{\nu} \approx 10^{-13} \text{ cm}^{-2} \text{ s}^{-1}$ . At this energy the probability that a neutrino converts into a muon within the range of the detector is  $\approx 10^{-4}$ . The number of detectable muons is  $\approx 3$  per  $\text{km}^2$  per year. This number scales roughly with the luminosity of the source and the inverse of the distance squared. The estimate only takes into account muon events from  $\nu_{\mu}$ 's produced directly in  $\pi$  decay. We have also made a more detailed estimate that convolutes the neutrino flux with the probability of neutrino detection through both muon and shower observation, taking into account the absorption of the neutrino flux while passing through the Earth (see for instance Appendix C in [19]), and assuming that after propagation from the source neutrinos have oscillated so that the flavor ratio is  $\nu_e : \nu_{\mu} : \nu_{\tau} = 1 : 1 : 1$ . We obtain a muon event rate  $N_{\mu} \approx 9 \text{ km}^{-2} \text{ yr}^{-1}$  and a shower rate  $N_{\text{sh}} \approx 2 \text{ km}^{-2} \text{ yr}^{-1}$  for an AGN located at a zenith an-



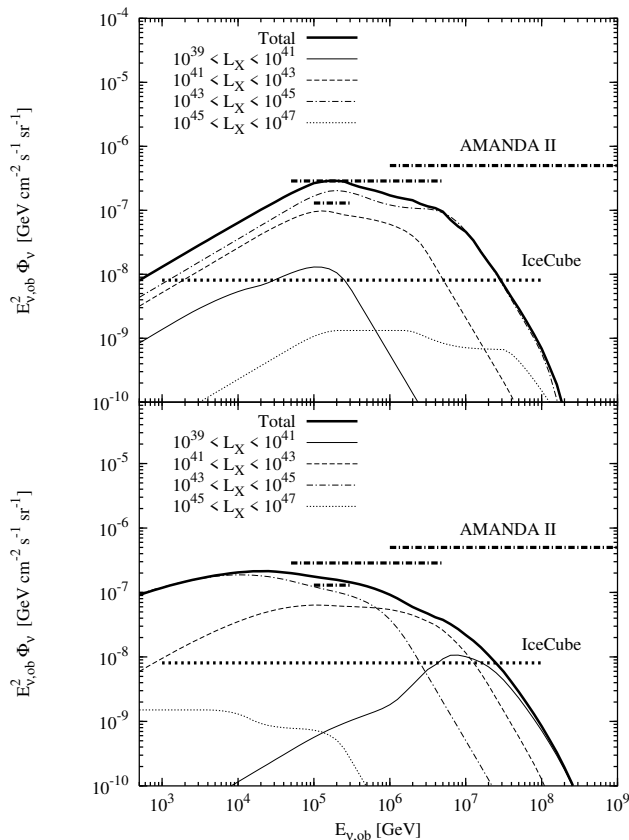


FIG. 5: Radio-quiet AGN diffuse  $\nu_{\mu} + \bar{\nu}_{\mu}$  flux reaching Earth (thick solid line). The fact that half of the muon neutrinos disappear due to oscillations is accounted for. The contribution to the total neutrino flux (thick lines) from radio-quiet AGNs in different X-ray luminosity bins (in  $\text{erg s}^{-1}$ ) is shown in thin lines. The top panel shows the results of a calculation where the black hole mass is varied, while the bottom panel shows the case where the accretion rate is varied (see text for details). Also shown are the latest AMANDA II limits on an  $E_{\nu}^{-2}$  diffuse  $\nu_{\mu} + \bar{\nu}_{\mu}$  flux which apply in different energy ranges (thick dashed-dotted lines) [15, 16], and the expected IceCube sensitivity after 1 year of operation (for an  $E_{\nu}^{-2}$  diffuse  $\nu_{\mu} + \bar{\nu}_{\mu}$  flux at 90% C.L.) [5] (thick dashed line).

gle 90 degrees (with respect to the vertical direction) in a detector such as Icecube at an average depth of  $\sim 1.8$  km water equivalent. The muon and shower energy threshold we used is 500 GeV.

For the diffuse fluxes plotted in Fig. 5 we predict a muon rate integrated over the  $2\pi$  northern sky (where the background due to atmospheric muons is negligible) of the order of a few hundred events and a shower rate about 3 times smaller, with roughly the same rate for the fixed  $M_{\text{BH}}$  case. IceCube can also identify events coming from the southern hemisphere despite the large muon background by selecting events with high enough energy [5, 20]. The number of muon events expected in this model from the  $2\pi$  southern sky for an energy threshold of  $10^6$  GeV is  $N_{\mu} \approx 17 \text{ km}^{-2} \text{ yr}^{-1}$  for the variable  $M_{\text{BH}}$  case and  $N_{\mu} \approx 8 \text{ km}^{-2} \text{ yr}^{-1}$  for the fixed  $M_{\text{BH}}$  case.

## V. SUMMARY AND CONCLUSIONS

We have investigated the high energy neutrino emission from radio-quiet AGNs, which is the most numerous class of AGNs. The neutrino emission in these AGNs, which lack prominent jets, is attributed to  $p\gamma$  and  $pp$  collisions of relativistic protons accelerated in shocks occurring near the central black hole, which are also responsible for a core component of the observed X-ray luminosity. The calculations were performed for a specific model of the AGN core in which an abortive jet leads to collisions of blobs inside the inner edge of the accretion disk. The results, however, should be generic to any model involving particle acceleration in the inner region of the accretion flow, e.g. [7, 8]. This model allows us to predict spectral details whose features depend on physical parameters related to the black hole mass, accretion rate and X-ray/UV luminosity, as well as shock physics parameters such as proton injection fraction, shock magnetic field strengths, etc. In particular, the model predicts muon and shower event rates from individual AGN, as a function of their observed X-ray/UV luminosity. The individual source event rates, as well as the corresponding diffuse fluxes are, for nominal parameters, already constrainable with AMANDA II, and should be strongly constrainable with the IceCube detector.

**Acknowledgments** We thank W.N. Brandt, F. Halzen, D.P. Schneider, S. Razzaque, E. Waxman and B. Zhang for discussions. This research is supported in part by NSF AST 0307376, the Monell foundation, and (for J.A.M) the Spanish “Ministerio de Educación y Ciencia” through the “Ramón y Cajal” program.

[1] See articles in *High Energy Processes in Accreting Black Holes*, eds. J. Poutanen and R. Svensson, *Ast. Soc. Pacific Conf. Series Vol. 161* (1999)  
 [2] F. Halzen and D. Hooper, *Rep. Prog. Phys.* **65**, 1025 (2002)  
 [3] A.A. Zdziarski, J. Poutanen and W.N. Johnson, *ApJ* **542**, 703 (2000)  
 [4] G. Ghisellini, F. Haardt and G. Matt, *Astron. & Astro-*

*phys.* **413**, 535 (2004)  
 [5] J. Ahrens *et al.*, *Astropart. Phys.* **20**, 507 (2004)  
 [6] S. Nayakshin, *Astrophys. J.* **540**, L37 (2000)  
 [7] D. Kazanas and D.C. Ellison, *ApJ* **304**, 178 (1986)  
 [8] F.W. Stecker and M.H. Salamon, *Sp. Sci. Rev.* **75**, 341 (1996)  
 [9] B.J. Boyle *et al.*, *Mon. Not. R. Astron. Soc.* **260**, 49 (1993)

- [10] N.I. Shakura and R.A. Sunyaev, *Astron. & Astrophys.* **24**, 337 (1973)
- [11] R. Walter and H.H. Fink, *Astron. & Astrophys.* **274**, 105 (1993)
- [12] S. Razzaque, P. Mészáros and E. Waxman, *Phys. Rev. D* **68**, 083001 (2003)
- [13] S. Razzaque, P. Mészáros and E. Waxman, *Phys. Rev. Lett.* **90**, 241103 (2003)
- [14] T.J. Turner and K.A. Pounds, *Mon. Not. R. Astron. Soc.* **240**, 833 (1989)
- [15] K. Woschnagg for the AMANDA Collaboration. Talk given at the 21<sup>st</sup> International Conference on Neutrino Physics and Astrophysics “Neutrino 2004”, Paris, France, June 2004
- [16] M. Ackermann *et al.*, *Astropart. Phys.* in press (2004)
- [17] J. Ahrens *et al.*, *Phys. Rev. Lett.* **90**, 251101 (2003)
- [18] J. N. Bahcall and E. Waxman, *Phys. Rev. D* **59**, 023002 (1999); *Phys. Rev. D* **64**, 023002 (2001)
- [19] D. Guetta *et al.*, *Astropart. Phys.* **20**, 429 (2004)
- [20] J. Alvarez-Muñiz and F. Halzen, *Phys. Rev. D* **63**, 037302 (2001)